Lasers in Surgery and Medicine 37:155–160 (2005)

Modeling and Simulations of the Pharmacokinetics of Fluorophore Conjugated Antibodies in Tumor Vicinity for the Optimization of Fluorescence-Based Optical Imaging

G. Fibich,[1] A. Hammer,[2] G. Gannot,[3] A. Gandjbakhche,[4] and I. Gannot[2,4]*
[1]*Department of Applied Mathematics, Faculty of Exact Sciences, Tel-Aviv University, Tel-Aviv 69978, Israel*
[2]*Department of Biomedical Engineering, Faculty of Engineering, Tel-Aviv University, Tel-Aviv 69978, Israel*
[3]*Laboratory of Pathology and Urologic Oncology Branch, National Cancer Institute, National Institutes of Health, Gaithersburg, Maryland 20877*
[4]*Laboratory of Integrative and Medical Biophysics, National Institutes of Health, Bethesda, Maryland 20892*

Background and Objectives: One of the methods to detect and localize tumors in tissue is to use fluorophore conjugated specific antibodies as tumor surface markers. The goals of this study are to understand and quantify the pharmacokinetics of fluorophore conjugated antibodies in the vicinity of a tumor. This study concludes another stage of the development of a non-invasive fluorescenated antibody-based technique for imaging and localization of tumors in vivo.

Study Design/Materials and Methods: A mathematical model of the pharmacokinetics of fluorophore conjugated antibodies in the vicinity of a tumor was developed based on histological staining experiments. We present the model equations of concentrations of antibodies and free binding sites. We also present a powerful simulation tool that we developed to simulate the imaging process. We analyzed the model and studied the effects of various independent parameters on the imaging result. These parameters included initial volume of markers (injected volume), total number of binding sites, tumor size, binding and dissociation rate constants, and the diffusion coefficient. We present the relations needed between these parameters in order to optimize the imaging results.

Results and Conclusions: A powerful and accurate tool was developed which may assist in optimizing the imaging system results by setting the injection volume and concentration of fluorophore conjugated antibodies in tissue and approximating the time interval where maximum specific binding occurs and the tumor can be imaged. Lasers Surg. Med. 37:155–160, 2005. © 2005 Wiley-Liss, Inc.

Key words: modeling; optical imaging; pharmacokinetics; diagnosis

INTRODUCTION

Imaging and localization of a tumor is a key step in determining optimal therapy. Imaging may detect very early stages of transitions in the cell. It can also monitor tumor progression or regression in response to treatment.

Fluorescenated antibody imaging technique is based on antigen-antibody systems with high specificity. The antibodies are used as specific marking agents for the antigen and are visible when tagged with a tracer.

Fluorescenated antibody imaging technique has distinct advantages over common imaging techniques. This wide range application method offers a variety of functional imaging modalities, while avoiding the disadvantages of radio-labeled based imaging, such as ionization, excitation, breaking of molecular bonds, chemical changes, and biological changes. Furthermore, the availability of fluorophores and the ability to conjugate them to antibodies make the method relatively low cost, portable and available at the patient's bedside. The constant development of new fluorophores, together with advances in the understanding the antigens specific to a tumor, make this method very powerful and attractive.

These non-invasive "optical biopsies," if successful, can assist in minimizing sampling errors in invasive destructive biopsies and in the future may replace them. This method has also the ability to monitor disease progression or regression in response to therapy.

The imaging technique that we are currently working on is based on "Anti-CD3" antibodies conjugated to a fluorescent marker (FITC or IRD38) [1], injected to the tumor area, and specifically bind to receptors on T cells ("sites") as shown in Figure 1. These T cells reach the tumor area as part of the natural immune system reaction of the object to a cancerous tumor [2]. After injecting the markers, external laser excitation is applied, and the fluorescence of the markers is monitored using the setup [3,4] described in Figure 2. The anesthetized experimental object is held on a custom-designed device (to avoid movement of the head) mounted on an XYZ positioner. After injecting the markers, they are excited by a CW laser beam—usually a Ti sapphire

Contract grant sponsor: Society for Lasers in Medicine and Surgery.
*Correspondence to: I. Gannot, Laboratory of Integrative and Medical Biophysics, National Institutes of Health, Bethesda, MD 20892. E-mail: gannoti@mail.nih.gov
Accepted 10 May 2005
Published online 21 July 2005 in Wiley InterScience (www.interscience.wiley.com).
DOI 10.1002/lsm.20200

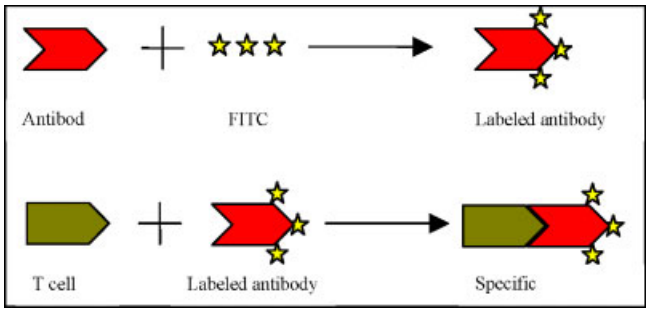

Fig. 1. The imaging method diagram: The imaging process includes labeling an antibody with a marker such as FITC, then injecting the labeled antibody ("marker") into the tissue, and waiting until it naturally binds to the TCR (T cell receptor) and tags the tumor boundary. [Figure can be viewed in color online via www.interscience.wiley.com.]

laser (Millenia, Spectra physics Lasers) at 778 nm (optimized to the IRD-38 absorption line). The laser beam is directed to the tissue through sets of reflecting mirrors. The emitted fluorescent light (maximum emission at 806 nm) is limited by special band pass filters (Omega filters, Cat. No. 835DF70, 800–875 nm). The filters suppress the laser signal while being transparent to the returning fluorescence signal, which is collected by a high precision fluorescent camera (MicroMAX, Roper Scientific, Trenton, NJ). The data is collected and the location is reconstructed [3,4] using an image processing tool.

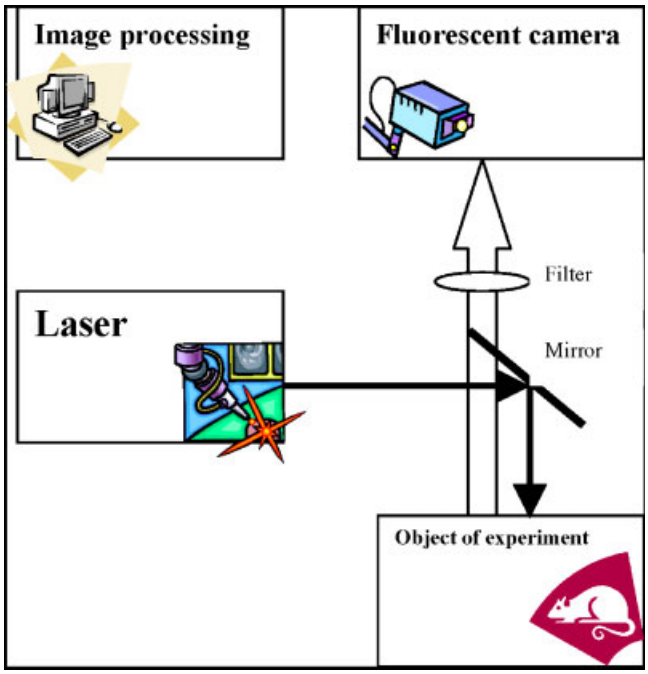

Fig. 2. The imaging procedure setup diagram: The anesthetized experimental object is held on a custom-designed device. We are using excitation by a CW Ti-Sapph laser at 778 nm, and a set of filters and mirrors as shown. [Figure can be viewed in color online via www.interscience.wiley.com.]

The fluorescence images are then analyzed by our theoretical model and the tumor location is extracted. In healthy and sick subjects, the clearance time is significantly different. It is expected that the existence of the tumor will interfere with normal clearing of the markers and therefore the fluorescence signal will decline significantly slower than the fluorescence signal of the healthy subjects [5,6,8–10]. This method is general and dye can easily be replaced by IR agents (as we already do now in phantoms and in in vivo studies [10,11]). Antibodies can also be replaced according to the specificity to other tumor markers.

RESEARCH MOTIVATION

Successful implementation of imaging based on fluorescenated antibodies depends on the answers to many questions, such as: Which marker should be used? What initial concentration of markers is optimal? What are the diffusion, binding, and dissociation rate constants? Empirically, it is impossible to find out the exact combination of parameters that will lead to maximal specific signal, pointing to the tumor, while minimizing the noise being generated by free markers.

The main object of this research was therefore to construct a mathematical model for the imaging method and use this model to find the best combination of parameters to achieve optimized imaging results.

MODEL OVERVIEW

We have broadly investigated the imaging method, as was described in the previous section. We identified the main processes of the imaging method which are:

(a) Diffusion of markers from injection area to the tissue and tumor area.
(b) Binding of markers to sites.
(c) Dissociation of markers from sites.

Morrison et al. [7] presented a diffusion-reaction model that accounts for transport of substances through tissues and probe membranes, and also accounts for transport across the microvasculature.

Praxmarer et al. [8] presented an improved computational model for investigating monoclonal antibody-based protocols for diagnostic imaging and therapy of solid tumors. Even though it was intended to be used in the radio labeling imaging method, this model was a good basic model to start from, when dealing with fluorescenated antibodies imaging.

In our model, we have located the binding sites in a volume layer around the tumor surface as shown in Figure 3. This assumption was based on data from histological staining experiments that we conducted, an example is shown in Figure 4. The model includes a partial differential equation which describes the temporary and volumetric changes in the concentration of markers (Eq. 1.1) and

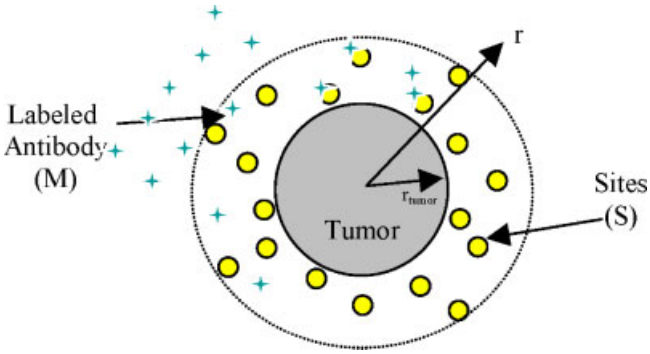

Fig. 3. The model diagram: Binding sites (small circles) are located in a thin volume layer (dashed line) around the tumor (shaded circle). Binding and dissociation of markers (small star signs) take place all over the volume layer. [Figure can be viewed in color online via www.interscience.wiley.com.]

another differential equation which describes the changes in the concentration of sites available for binding in the volume layer (Eq. 1.2).

Model Equations

The free marker concentration is determined by:

$$\frac{\partial M(r,t)}{\partial t} = D\nabla^2 M(r,t) + K_{\mathrm{d}}[S_{\mathrm{total}}(r) - S(r,t)] - K_b M(r,t) S(r,t) \quad (1.1)$$

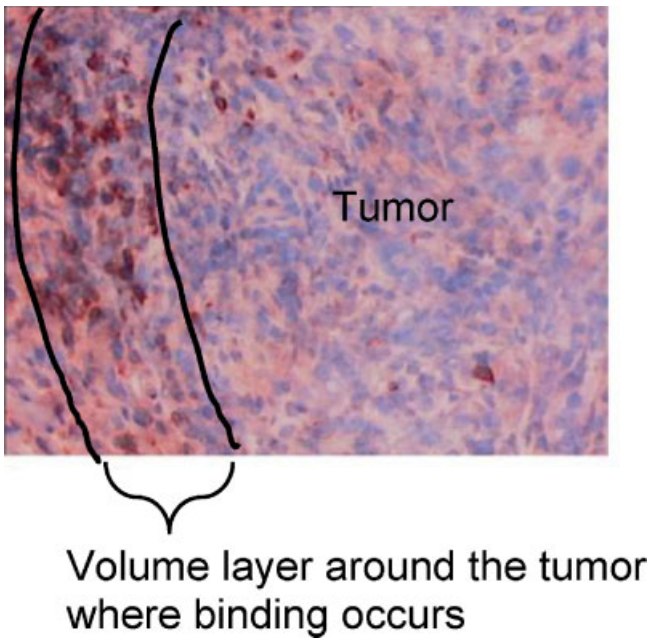

Fig. 4. Histological staining: 5-day-old tumor with CD-3 at magnitude 200×. A volume layer where binding was detected can be seen on the left. [Figure can be viewed in color online via www.interscience.wiley.com.]

for $r > r_{\mathrm{tumor}}$, where D is the diffusion coefficient, K_{b} is the binding rate constant, K_{d} is the dissociation rate constant, $S_{\mathrm{total}}(r)$ denotes the initial sites concentration at the volume layer.

The concentration of sites is determined by:

$$\frac{\partial S(r,t)}{\partial t} = K_{\mathrm{d}}[S_{\mathrm{total}}(r) - S(r,t)] - K_{\mathrm{b}} M(r,t) S(r,t) \quad (1.2)$$

On the tumor surface this model includes a "no flux" boundary condition:

$$M_r(r_{\mathrm{tumor}}, t) = 0 \quad (1.3)$$

Here r_{tumor} is the radius of the tumor.

RELATIONS BETWEEN THE IMAGING METHOD PARAMETERS

Using dimensional analysis, we have reduced the initial number of dimensional parameters: S_{total}, M_0, D, K_{b}, K_{d}, r_{tumor} to only three non-dimensional combinations, where M_0 is the free marker concentration at time 0.

The non-dimensional binding rate constant is:

$$K_{\mathrm{b}}^* = K_{\mathrm{b}} t_{\mathrm{D}} S_{\mathrm{total}} \quad (1.4)$$

The non-dimensional dissociation rate constant is:

$$K_{\mathrm{d}}^* = K_{\mathrm{d}} t_{\mathrm{D}} \frac{S_{\mathrm{total}}}{M_0} \quad (1.5)$$

The ratio of concentration of markers to sites is:

$$\mathrm{R}^* = \frac{M_0}{S_{\mathrm{total}}} \quad (1.6)$$

Note that t_{D} is the diffusion process time. We have chosen t_{D} to serve as the characteristic time of the problem. We have determined the timing relations that are needed in order to achieve the ideal timing frame for the optimal imaging result:

$$T_{\mathrm{binding}} << T_{\mathrm{diffusion}} << T_{\mathrm{dissociation}} \quad (1.7)$$

We substituted the non-dimensional constants in Equations (1.4), (1.5), and (1.6) into the timing relations (Eq. 1.7) in order to find the constants relations for optimal imaging result:

$$\frac{1}{K_{\mathrm{b}}} << \frac{S_{\mathrm{total}} r_{\mathrm{tumor}}^2}{D} << \frac{M_0}{K_{\mathrm{d}}} \quad (1.8)$$

SIMULATION TOOL AND THE DETECTION PROCEDURE

Simulation Tool

We have developed a one-dimensional simulation tool based on radial symmetry. Due to the non-linearity of the problem, there are no exact analytical solutions. So, in order to verify our simulations, we have constructed two different numerical schemes: an implicit scheme and an explicit scheme.

We have done various simulations, in order to study the influence of every parameter on the imaging result. We

have also simulated the influence of the values and relations of the three non-dimensional combinations as produced by the dimensional analysis. We have used the optimal relation produced by the analysis (Eq. 1.8) and verified it by comparing simulations results with different correlations to this relation.

Figures 5 and 6 show simulation results for the free markers concentration and the free sites concentration, respectively. These simulations are conducted with and without binding sites, and also at 0.4 mm from the tumor boundary. The dotted line in Figure 5 shows the solution of free markers concentration at the boundary of a tumor, as a function of time, with no binding sites.

We can see that the markers concentration decreases and simply because of the diffusion process. The solid line in Figure 5 shows the solution of the same model when there are binding sites. This is the free markers concentration at the boundary of the tumor as a function of time. We can see that there is a noticeable difference between these two results. This difference is due to the binding of free markers to sites, which results in additional reduction of the free markers concentration near the tumor boundary. The dashed line shows the concentration of free markers at 0.4 mm from tumor boundary, as a function of time. We can see that the concentration of free markers at this location is lower than the concentration near the tumor boundary.

In Figure 6, we present the simulation result of the free sites concentration at the boundary of the tumor, as a function of time. The free sites concentration decreases due to the binding of markers to these sites. The initial

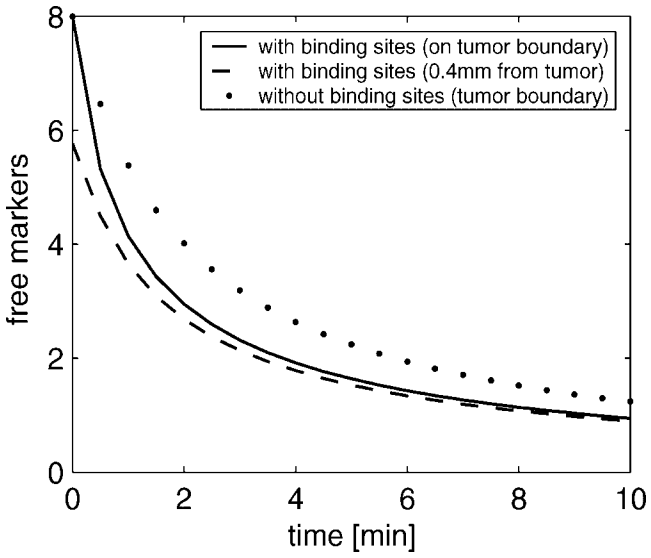

Fig. 5. Free markers concentration: The imaging technique model simulation result of free markers concentration when the tumor has binding sites: on the tumor boundary (solid line), 0.4 mm from the tumor boundary (dashed line), and when the tumor has no binding sites (dotted line).

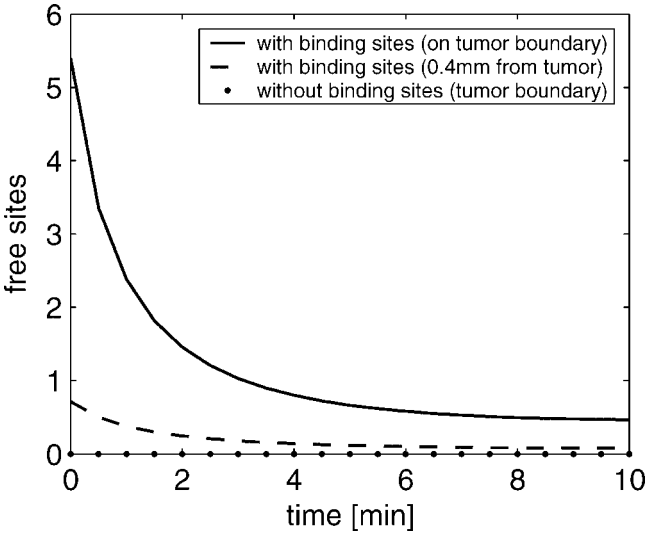

Fig. 6. Free sites concentration: The imaging technique model simulation result of free sites concentration when the tumor has binding sites—on the tumor boundary (solid line), 0.4 mm from the tumor boundary (dashed line), and when the tumor has no binding sites (dotted line).

concentration of binding sites is determined by the distribution function:

$$g(r;a) = F\left(\frac{r - r_{\text{tumor}}}{a}\right) \tag{1.9}$$

where r_{tumor} is the tumor radius, and r is the distance from the center of the tumor. Generally F is an exponential function and a is the width parameter. We can see that the relation of initial markers concentration, total sites concentration, and the binding rate constant that we have chosen results in binding of almost 90% of the binding sites to markers in less than 60% of the experiment duration. We also notice the difference between the tumor boundary result and the result at 0.4 mm from the tumor boundary, where there are fewer sites available and therefore the binding process has less influence.

Total signal measurements at the boundary of the tumor, as a function of time, are presented in Figure 7. This is the practical measurement of our imaging procedure. The differences between the simulation of a tissue and a tumor with binding sites, and the simulation of a tissue and a tumor without binding sites are clearly shown here. When there are no binding sites, total signal intensity decreases by 85%. When there are binding sites, due to the binding of markers to sites, the total signal dropped by only 20% after 10 minutes. As for localization of the tumor, we can also see the differences between the tumor boundary signal and the signal at 0.4 mm from the boundary, which has dropped 60% of its initial value—these differences allow us to evaluate the position of the tumor boundaries.

In Figure 8, we present a simulation of the practical outcome of this work. We implemented the optimal relations we found as presented in Equation (1.8). In this

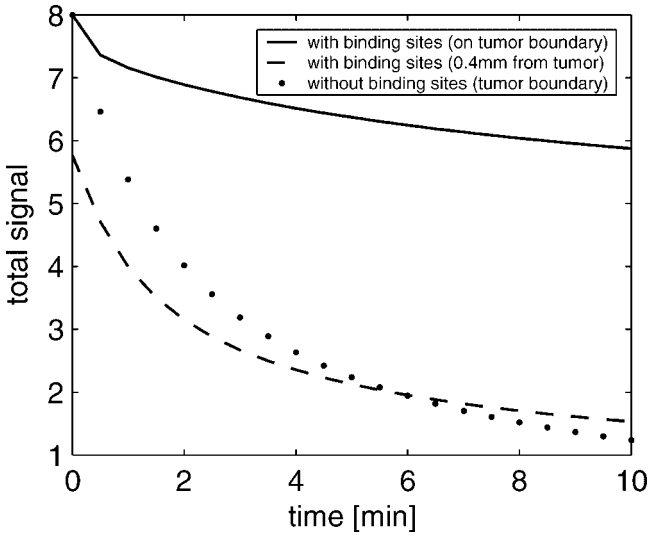

Fig. 7. Total emitted signal: Imaging technique model simulation result of the total emitted signal when the tumor has binding sites: (solid line) on the tumor boundary, (Dashed line) 0.4 mm from the tumor boundary, (Dotted line) Tumor has no binding sites.

figure, we present a series of two-dimensional images, which show the total fluorescent signal as a function of radial distance from the tumor center, at specific times. When comparing the simulation of the tumor with binding sites (left column) and the simulation of the tumor without binding sites (right column), we can see a significant difference after 5 minutes. This way, simulations and imaging results can be used to differentiate sick tissue from healthy tissue, similarly a cancerous tumor from a benign one and also locate the position of a cancerous tumor, if there is one.

DISCUSSION CONCLUSIONS AND FUTURE DIRECTIONS

The results of the current research are useful for finding the exact combination of parameters that will lead to maximal specific signal and assessment of tumor location deep beneath the tissue, while minimizing the noise being generated by free, unbound markers. The mathematical model presented is quite complicated so we made several preliminary assumptions in order to simplify the model and make it useful for diagnostic planning.

Mathematical Model Aspects

Our initial assumption was that the diffusion of markers could only occur in the tissue surrounding the tumor. This

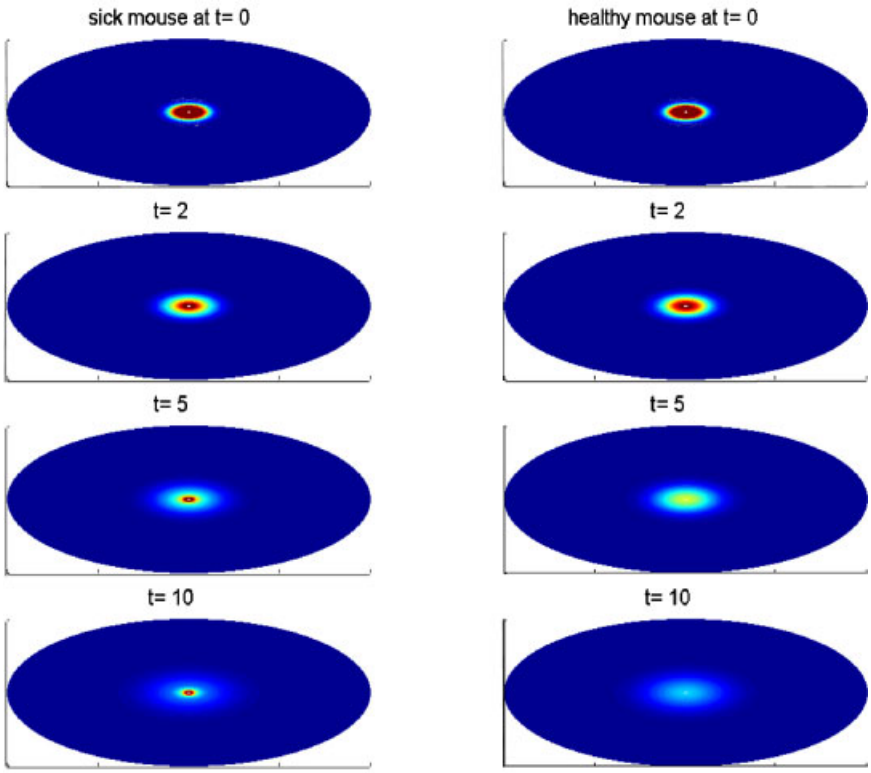

Fig. 8. Complete imaging method simulation: The complete imaging method simulation based on 1D radial symmetry model simulations. When comparing the simulation of tumor with binding sites (left column) and the simulation of tumor without binding sites (right column) we can see a significant difference after 5 minutes. [Figure can be viewed in color online via www.interscience.wiley.com.]

assumption holds true for small dense tumors and is also adequate for larger ones. In future research, we plan to upgrade the model and include also diffusion into the tumor.

In our present model, we disregard the uptake of markers by the systemic and the lymphatic. We estimate that the influence of uptake by the systemic is negligible due to a much slower characteristic time. However, due to injection of a large volume, hydrostatic pressure is formed, and there is a significant lymphatic drainage. In future research, we plan to include clearance by the lymphatic system in our model and study the effect of this process on the rate constants.

Experimental Work Aspects

In the present research, we gave little importance to the position of the markers injection point. This assumption was based mainly on injection of large volumes. In future studies, we plan to repeat the experiments while measuring the position of the injection point to study the influence on our imaging results.

We also plan to reconsider two other aspects of the injection procedure, the volumes and rates. In the present research, we have learned that the injection volumes were very large compared to the tumor and the tissue surrounding it. We did some experiments reducing the injection volumes from the initial 50 μl injection to 5 μl. This was the minimal volume that allowed us a sufficient signal to noise ration (SNR) for the imaging result. We plan to further reduce these volumes, with the need to lower noise and improve the sensitivity of the fluorescence camera.

The second issue we plan to study is the influence of injection rate on the diffusion and clearance of markers. When studying comparable injection procedures from other tissues, such as brain tissue, scientists use injection rates of parts of μl per minute. Our current rate is much higher, and we do not yet have a method to measure it precisely.

We have conducted several immune-histochemical staining experiments (mainly Hematoxylin and Eosin staining) in order to understand what the boundary of the tumor looks like, and where the T cells are located around the tumor. The model that we have developed is based on analyzing the results of these experiments. We plan to repeat the staining experiments in different stages of the complete imaging procedure, and we plan to investigate the existence of "pools" of markers created by the injection, diffusion of markers into the tumor area, and to study further the influence of the injection point on markers concentration.

SUMMARY

In this work we have constructed a mathematical model to describe diffusion, binding, and dissociation of markers, and sites in healthy tissue and in tissue with a tumor. We have determined the relations between the method parameters in order to achieve optimized imaging results. We have constructed a reliable simulation tool, using both implicit and explicit schemes to verify our numerical code. Using the simulation results, we have shown that choosing the imaging method parameters based on the relation that we have found leads to the ability to identify and localize a tumor in the inspected tissue.

ACKNOWLEDGMENTS

Mr. Amit Hammer thank the Society for Lasers in Medicine and Surgery for its support through a summer research grant.

REFERENCES

1. Hamster Anti-Mouse CD3 Data Sheet—Southern Biotechnology Association, Inc. 2001.
2. Gannot G, Gannot I, Buchner A, Vered H, Keisari Y. Increase in immune cell infiltration with progression of oral epithelium from hyperkeratosis to dysplasia and carcinoma. Br J Cancer 2002;86(9):1444–1448.
3. Gannot I, Gandjbakhche AH, Gannot G, Fox PC, Bonner RF. Optical simulations experiments for development of a non-invasive technique for the diagnosis of diseased salivary glands *in situ*. Med Phys 1998;27(7):1139–1144.
4. Gannot I, Garashi A, Gannot G, Chernomordik V, Gandjbakhche A. Quantitative 3-D imaging of tumor labeled with exogenous specific fluorescence markers Appl Opt 2003; 42(15):3073–3080.
5. Gandjbakhche AH, Weiss GH. Random walk and diffusion-like models of photon migration in turbid media Prog Opt 1995;XXXIV(V):335–402.
6. Chermomordik V, Hattery D, Gannot I, Gandjbakhche AH. Inverse Method 3-D Reconstruction of Localized *in-vivo* Fluorescence-Application to Sjogren's Syndrome. IEEE J Selected Top Quantum Electron 1999;5:930–935.
7. Morrison PF, Bungay PM, Hsiao JK, Ball BA, Mefford IN, Dedrick RL. Quantitative microdialysis: Analysis of transients and application to pharmacokinetics in brain. J Neurochem. 1991;57:103–119.
8. Praxmarer M, Sung C, Bungay PM, van Osdol WW. Computational models of antibody-based tumor imaging and treatment protocols. Ann Biomed Eng. 2001;29(4):340–358.
9. Gannot I, Gannot G, Garashi A, Gandjbakhche A, Buchner A, Keisari Y. Laser activated fluorescence measurements and morphological features—An in vivo study of clearance time of FITC tagged cell markers. J Biomed Opt 2002;7:14–19.
10. Gannot I, Garashi A, Chernomordik V, Gandjbakhche A. Quantitative optical imaging of pharmacokinetics of specific fluorescent tumor markers through turbid media such as tissue. Opt Letters 2004;29(7):742–744.
11. Gannot I, Izhar R, Hekmat F, Chernomordik V, Gandjbakhche A. Functional optical detection based on pH dependent fluorescence lifetime J Lasers Med Surg 2004; 35(5):342–348.